nature physics

ARTICLES

https://doi.org/10.1038/s41567-020-1008-4

Underground test of gravity-related wave function collapse

Sandro Donadi[1]✉, Kristian Piscicchia[2,3]✉, Catalina Curceanu[3], Lajos Diósi[4], Matthias Laubenstein[5] and Angelo Bassi[6,7]✉

Roger Penrose proposed that a spatial quantum superposition collapses as a back-reaction from spacetime, which is curved in different ways by each branch of the superposition. In this sense, one speaks of gravity-related wave function collapse. He also provided a heuristic formula to compute the decay time of the superposition—similar to that suggested earlier by Lajos Diósi, hence the name Diósi–Penrose model. The collapse depends on the effective size of the mass density of particles in the superposition, and is random: this randomness shows up as a diffusion of the particles' motion, resulting, if charged, in the emission of radiation. Here, we compute the radiation emission rate, which is faint but detectable. We then report the results of a dedicated experiment at the Gran Sasso underground laboratory to measure this radiation emission rate. Our result sets a lower bound on the effective size of the mass density of nuclei, which is about three orders of magnitude larger than previous bounds. This rules out the natural parameter-free version of the Diósi–Penrose model.

Quantum mechanics beautifully accounts for the behaviour of microscopic systems, while in an equally beautiful but radically different way classical mechanics accounts for the behaviour of macroscopic objects. The reason why the quantum properties of microscopic systems—most notably, the possibility of being in the superposition of different states at once—do not seem to carry over to larger objects has been the subject of a debate that is as old as quantum theory itself, as exemplified by Schrödinger's cat paradox[1].

It has been conjectured that the superposition principle, the building block of quantum theory, progressively breaks down when atoms glue together to form larger systems[2–7]. The reason is that the postulate of wave function collapse (introduced by von Neumann, and now part of the standard mathematical formulation of the theory, according to which the quantum state of a system suddenly collapses at the end of a measurement process), though very effective in describing what happens in measurements, clearly has a phenomenological flavour. There is no reason to believe that measurements are so special as to temporarily suspend the quantum dynamics given by the Schrödinger equation and replace it with a completely different one. More realistically, if collapses occur at all, they are part of the dynamics: in some cases, they are weak and can be neglected; in some other cases, such as in measurements, they become strong and rapidly change the state of a system. Decades of research in this direction has produced well defined models accounting for the collapse of the wave function and the breakdown of the quantum superposition principle for larger systems[5,8–10], and now the rapid technological development has opened the possibility of testing them[11]. One question is left open: what triggers the collapse of the wave function?

In his lectures on gravitation, Feynman discusses how a breakdown of the quantum superposition principle at a macroscopic scale leaves open the possibility that gravity might not be quantized[12]. Along this line of thinking, Penrose (and Diósi, independently) suggested that gravity, whose effects are negligible at the level of atoms and molecules, but increase substantially at the level of macroscopic objects, could be the source of the wave function collapse: "My own point of view is that as soon as a 'significant' amount of space-time curvature is introduced, the rules of quantum linear superposition must fail"[13]. When a system is in a spatial quantum superposition, a corresponding superposition of two different spacetimes is generated, as illustrated in Fig. 1. Penrose then gives arguments[14–16] as to why nature 'dislikes' and, therefore, suppresses superpositions of different spacetimes; the more massive the system in the superposition, the larger the difference in the two spacetimes and the faster the wave function collapse.

Even without proposing a detailed mathematical model, Penrose provides a formula that estimates, in non-relativistic and weak-gravitational-field limits, the expected time τ_{DP} of the collapse of a quantum superposition[14]:

$$\tau_{\mathrm{DP}} = \frac{\hbar}{\Delta E_{\mathrm{DP}}} \tag{1}$$

where ΔE_{DP} measures how large, in gravitational terms, the superposition is. Given a system with mass density $\mu(\mathbf{r})$, in the simple case of the centre of mass being in a superposition of two states displaced by a distance $\mathbf{d}$,

$$\Delta E_{\mathrm{DP}}(\mathbf{d}) = -8\pi G \int \mathrm{d}\mathbf{r} \int \mathrm{d}\mathbf{r}' \frac{\mu(\mathbf{r})[\mu(\mathbf{r}'+\mathbf{d}) - \mu(\mathbf{r}')]}{|\mathbf{r}-\mathbf{r}'|} \tag{2}$$

Equations (1) and (2), which are valid in the Newtonian limit, were previously proposed by Diósi[17,18], following a different approach. For a point-like $\mu(\mathbf{r}) = m\delta(\mathbf{r}-\mathbf{r}_0)$, with m the mass of the particle and δ the Dirac delta distibution, equation (2) diverges because of the $1/r$ factor, leading to an instantaneous collapse, which is clearly wrong. To avoid this problem, one has to smear the mass density. This is

[1]Frankfurt Institute for Advanced Studies (FIAS), Frankfurt am Main, Germany. [2]Centro Fermi - Museo Storico della Fisica e Centro Studi e Ricerche "Enrico Fermi", Rome, Italy. [3]INFN, Laboratori Nazionali di Frascati, Frascati, Italy. [4]Wigner Research Centre for Physics, Budapest, Hungary. [5]INFN, Laboratori Nazionali del Gran Sasso, Assergi, Italy. [6]Department of Physics, University of Trieste, Trieste, Italy. [7]INFN, Sezione di Trieste, Trieste, Italy.
✉e-mail: donadi@fias.uni-frankfurt.de; kristian.piscicchia@cref.it; abassi@units.it

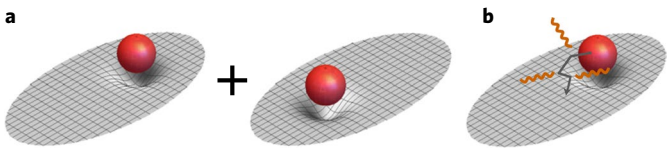

Fig. 1 | The Diósi–Penrose (DP) model of gravity-related wave function collapse. a, According to quantum gravity, a spatial quantum superposition of a system (red sphere) generates a superposition of different spacetime curvatures (grey sheets), corresponding to the possible different locations of the system. Penrose argues that a superposition of different spacetimes is unstable and decays in time, making the system's wave function also collapse. He provides an estimate for the time of collapse as given in equation (1), which is faster for a larger system, similar to that suggested earlier by Diósi. **b**, The master equation of the DP model (equation (3)) predicts not only the collapse of the wave function, but also an omnipresent Brownian-like diffusion (represented by the grey arrow) for each constituent of the system. When the constituents are charged (protons and electrons), the diffusion is accompanied by the emission of radiation (wavy orange lines), with a spectrum that depends on the configuration of the system. This is given by equation (4) in the range $\Delta E = (10\text{–}10^5)$ keV of photon energies. The predicted radiation emission is faint but potentially detectable by an experiment performed in a very low-noise environment. We performed such an experiment to rule out the original parameter-free version of the DP model.

implemented in different ways by Diósi and Penrose. Diósi suggests introducing a new phenomenological parameter, measuring the spatial resolution of the mass density[19,20]; Penrose instead suggests that the mass density of a particle is given by $\mu(\boldsymbol{r}) = m|\psi(\boldsymbol{r},t)|^2$ (ref. [15]), where $\psi(\boldsymbol{r},t)$ is a stationary solution of the Schrödinger–Newton equation[21,22]. For either choice, we will call the size of the particle's mass density R_0.

A direct test of equation (1) requires creating a large superposition of a massive system, to guarantee that τ_{DP} is short enough for the collapse to become effective before any kind of external noise disrupts the measurement (see ref. [23] for an alternative approach). One of the first proposals in this direction was put forward by Penrose himself and collaborators[24], who suggested a set-up for creating a spatial superposition of a mirror of mass $\sim 10^{-12}$ kg that, according to equation (2), has a decay time of order $\tau_{\mathrm{DP}} \simeq 0.002\text{–}0.013$ s (Supplementary Information), which is competitive with standard decoherence times. The major difficulty in implementing this and similar proposals consists in creating a superposition of a relatively large mass and keeping it stable for times comparable to τ_{DP}. To give some examples, the largest spatial superposition so far achieved[25] is about 0.5 m, but the systems involved are Rb atoms (mass $= 1.42 \times 10^{-25}$ kg), which are too light. In matter-wave interferometry with macromolecules[26], states are delocalized over distances of hundreds of nanometres, and masses beyond 25 kDa ($\sim 10^{-23}$ kg), but still not enough. By manipulating phononic states[27], collective superpositions of an estimated 10^{16} carbon atoms (mass $\sim 10^{-10}$ kg) are created over distances of 10^{-11} m, but the lifetime of phonons is of the order of $\sim 10^{-12}$ s, which is too short. These numbers show that keeping the superposition time, distance and mass large enough still poses huge technological challenges. Research towards creating larger and larger superpositions is very active[28–34], but further development is needed to reach the required sensitivity.

Here we show how to test gravitational-related collapse in an indirect way, by exploiting an unavoidable side effect of the collapse: a Brownian-like diffusion of the system in space. The reason is the following. Although Penrose refrains from proposing any detailed dynamics for the collapse, as suggested in refs. [14,15] and used explicitly in ref. [16], the simplest assumption is that the collapse is Poissonian, as for particle decay. This minimal requirement, together with the collapse time given in equations (1) and (2), implies the following Lindblad dynamics for the statistical operator $\rho(t)$ describing the state of the system (Supplementary Information):

$$\frac{\mathrm{d}\rho(t)}{\mathrm{d}t} = -\frac{i}{\hbar}[H,\rho(t)] - \frac{4\pi G}{\hbar}\int \mathrm{d}\mathbf{x}\int \mathrm{d}\mathbf{y}\,\frac{1}{|\mathbf{x}-\mathbf{y}|}\left[\hat{M}(\mathbf{y}),\left[\hat{M}(\mathbf{x}),\rho(t)\right]\right] \tag{3}$$

which is equivalent to the master equation derived in refs. [17,18]. The first term describes the standard quantum evolution while the second term accounts for the gravity-related collapse. In equation (3) H is the system's Hamiltonian and $\hat{M}(\mathbf{x}) = \sum_n \mu_n(\mathbf{x},\hat{\mathbf{x}}_n)$ gives the total mass density, with $\mu_n(\mathbf{x},\hat{\mathbf{x}}_n)$ the mass density of the nth particle, centred around $\hat{\mathbf{x}}_n$. Taking for example a free particle with momentum operator $\hat{\mathbf{p}}$, the contribution of the second term to the average momentum $\langle\mathbf{p}\rangle \equiv \mathrm{Tr}[\hat{\mathbf{p}}\rho]$ is zero, while the contribution to the average square momentum $\langle\mathbf{p}^2\rangle$ increases in time. This is diffusion.

This diffusion causes a progressive heating of the system[19], specifically a steady temperature increase. Assuming a mass distribution of the nuclei with an effective $R_0 \sim 10^{-15}$ m, the heating rate for a gas of non-interacting particles amounts to $\mathrm{d}T(t)/\mathrm{d}t = 4\sqrt{\pi}m_0 G\hbar/3k_{\mathrm{B}}R_0^3 \sim 10^{-4}\,\mathrm{K\,s^{-1}}$ (k_{B} is Boltzmann's constant and m_0 the nucleon mass), which is in contradiction with experimental evidence[35]. The value $R_0 \sim 10^{-14}$ m is also excluded by gravitational wave detection experiments[36]. However, neither result includes the possibility of dissipative effects, which are always associated with fluctuations, and may lead to equilibrium instead of a steady growth in temperature.

Whether at thermal equilibrium or not, particles will keep fluctuating under the collapse dynamics. Since matter is made up of charged particles, this process makes them constantly radiate. Therefore, a detection of the collapse-induced radiation emission is a more robust test of the model (cf. ref. [37]), even in the presence of dissipative effects.

Starting from equation (3), we computed the radiation emission rate, that is the number of photons emitted per unit time and unit frequency, integrated over all directions, in the range of wavelength $\lambda \in (10^{-5}\text{–}10^{-1})$ nm, corresponding to energies $E \in (10\text{–}10^5)$ keV. The reason for choosing this range can be understood in terms of a semi-classical picture: each time a collapse occurs, particles are slightly and randomly moved. This random motion makes them emit radiation, if charged. When their separation is smaller than λ, they emit as a single object with charge equal to the total charge, which can be zero for opposite charges as for an atom. In contrast, when their separation is larger than λ, they emit independently. Therefore, in order to maximize the emission rate, electrons and nuclei should be independent ($\lambda <$ atomic radius), while protons in the same nucleus should behave coherently ($\lambda >$ nuclear radius). This is achieved by considering the emission of photons with wavelength in the range mentioned above. In this range, the coherent emission of protons contributes with a term proportional to $(Ne)^2$ (N is the atomic number), while electrons contribute incoherently with a weaker term proportional to Ne^2. For this reason, and also because in the range of energies considered in our experiment the electrons are relativistic, while our derivation is not, to be conservative we will neglect the contribution of the electrons to the emission rate.

The photon emission rate $\mathrm{d}\Gamma_t/\mathrm{d}\omega_k$ per unit frequnecy ω_k is discussed in Methods and derived in Supplementary Information. The calculation is lengthy. In a nutshell, starting from equation (3), we compute the expectation value of the photon number operator at time t, that is $\langle a^\dagger_{\mathbf{k}\nu} a_{\mathbf{k}\nu}\rangle_t$, to the first perturbative order. By taking the time derivative, summing over the photon's polarizations ν and integrating over all the directions of the emitted photon, we eventually obtain

$$\frac{\mathrm{d}\Gamma_t}{\mathrm{d}\omega_k} = \frac{2}{3}\frac{Ge^2N^2N_{\mathrm{a}}}{\pi^{3/2}\varepsilon_0 c^3 R_0^3 \omega_k} \tag{4}$$

where G, e, ε_0 and c are constants of nature with the usual meaning and N_a is the total number of atoms. We leave R_0 as a free parameter to be bounded by experiments. Clearly, the number of emitted photons increases with N_a, as there are more protons affected by the noise. The factor N^2 accounts for the quadratic dependence on the atomic number, which substantially increases the predicted effect.

We performed a dedicated experiment to test this model of gravity-related collapse by measuring the spontaneous radiation emission rate from a germanium crystal and the surrounding materials in the experimental apparatus. The strong point of the experiment is that there was no need to create a spatial superposition, since according to equation (3) the collapse-induced diffusion and the associated photon emission occur for any state, including localized states of the system. The experiment was carried out in the low-background environment of the underground Gran Sasso National Laboratory of INFN. The Gran Sasso Laboratory is particularly suitable for high-sensitivity measurements of extremely low-rate physical processes, since it is characterized by a rock overburden corresponding to a minimum thickness of 3,100 m w.e. (metres water equivalent). The environmental emissions are generated by the rock radioactivity and the residual cosmic muon flux. Given that the cosmic radiation flux is reduced by almost six orders of magnitude, the main background source in the Gran Sasso Laboratory consists of γ-radiation produced by long-lived γ-emitting primordial isotopes and their decay products. They are part of the rocks of the Gran Sasso mountains and the concrete used to stabilize the cavity.

The set-up consisted of a coaxial p-type high-purity germanium detector surrounded by a complex shielding structure, with the outer part made of pure lead and the inner part made of electrolytic copper. The germanium crystal is characterized by a diameter of 8.0 cm and a length of 8.0 cm, with an inactive layer of 0.075 mm of lithium-doped germanium all around the crystal. The active germanium volume of the detector is 375 cm^3. The outer part of the passive shielding of the high-purity germanium detector consists of lead (30 cm from the bottom and 25 cm from the sides). The inner layer of the shielding (5 cm) is composed of electrolytic copper. The sample chamber has a volume of about 15 l ($(250\times250\times240)$ mm^3). The shield together with the cryostat are enclosed in an air-tight steel housing of 1 mm thickness, which is continuously flushed with boil-off nitrogen from a liquid nitrogen storage tank, in order to reduce the contact with external air (and thus radon) to a minimum. The experimental set-up is schematically shown in Fig. 2 (see also refs. [38,39]). The data acquisition system is a Lynx digital signal analyser controlled via GENIE 2000 personal computer software, both from Canberra-Mirion. In this measurement, the sample placed around the detector was 62 kg of electropolished oxygen-free high-conductivity copper in Marinelli geometry.

The measured emission spectrum, corresponding to a data-taking period of about 62 days (August 2014 and August 2015), is shown in Fig. 3, where emission lines generated by residual radionuclides present in the set-up materials are also visible. In particular, the region of the ^{60}Co lines (corresponding to the shaded green area highlighted in the total plot) is enlarged in the inset.

Data analysis was carried out to extract the probability distribution function (pdf) of the R_0 parameter of the model. Different from previous investigations[40,41], we perform not only the dedicated experiment but also an accurate Monte Carlo (MC) characterization, with a validated MC code based on the Geant4 software library, of the experimental set-up, which allowed us to compute the background originating from known sources, determining the contribution of each component of the set-up; the background simulation is described in greater detail in Methods. The residual spectrum was then compared with the theoretical prediction for the collapse-induced radiation, to extract a bound on R_0.

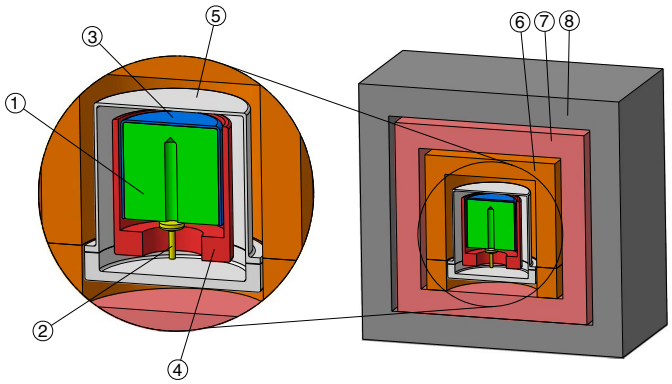

Fig. 2 | Schematic representation of the experimental set-up. The experimental apparatus is based on a coaxial p-type high-purity germanium detector, with the dimensions of 8.0 cm diameter and 8.0 cm length; the active volume is 375 cm^3. The detector is shielded by layers of electrolytic copper and pure lead. The inner part of the apparatus consists of the following main elements: 1, germanium crystal; 2, electric contact; 3, plastic insulator; 4, copper cup; 5, copper end-cup; 6, copper block and plate; 7, inner copper shield; 8, lead shield. In order to minimize the radon contamination an air-tight steel casing (not shown) encloses the shield and is continuously flushed with boil-off nitrogen from a liquid nitrogen storage tank.

The experimental and the MC simulated spectra agree to 88% in the energy range $\Delta E=(1{,}000–3{,}800)$ keV, whereas in the low-energy region there are larger deviations. This is mostly due to the impossibility of perfectly accounting for the residual cosmic rays and the bremsstrahlung caused by ^{210}Pb and its daughters in the massive lead shield. The energy range falls within the interval previously discussed for the validity of the theoretical model. Therefore, we take ΔE as the energy region of interest (ROI) for the following statistical analysis; the ROI is represented by the grey area in Fig. 3. In Fig. 4 the measured spectrum is compared, in the ROI, with the simulated background distribution. The total number of simulated background counts within ΔE is $z_b=506$ events, to be compared with the measured number $z_c=576$ events. The reason for this low rate is the fact that the detector set-up is especially designed for ultralow-background measurements. The spectrum in Fig. 3 only contains 'real' events, as the digital data acquisition system has a filter rejecting noise events by their pulse shape, with efficiency better than 99%.

Then, we estimated the number of signal events that would be measured during the acquisition time, generated in the materials of the apparatus as collapse-induced photons. To this end the detection efficiencies, which are shown, for the set-up components that give an appreciable contribution, in Supplementary Fig. 1, were taken into account.

Given the rate in equation (4) the expected signal contribution z_s, which is a function of the parameter R_0, turns out to be

$$z_s(R_0)=\sum_i\int_{\Delta E}\left.\frac{d\Gamma_t}{dE}\right|_i T\epsilon_i(E)\,dE=\frac{a}{R_0^3} \qquad (5)$$

where T is the total acquisition time of the experiment, $\epsilon_i(E)$ is the energy-dependent efficiency function for the ith component of the set-up and $a\sim1.8\times10^{-29}\,m^3$. By substituting the values z_c, z_b and z_s in the pdf of the parameter R_0 the following constraint is obtained:

$$R_0>0.54\times10^{-10}\ \text{m} \qquad (6)$$

with probability 0.95. The data analysis is extensively described in Supplementary Information, where the pdf is explicitly derived.

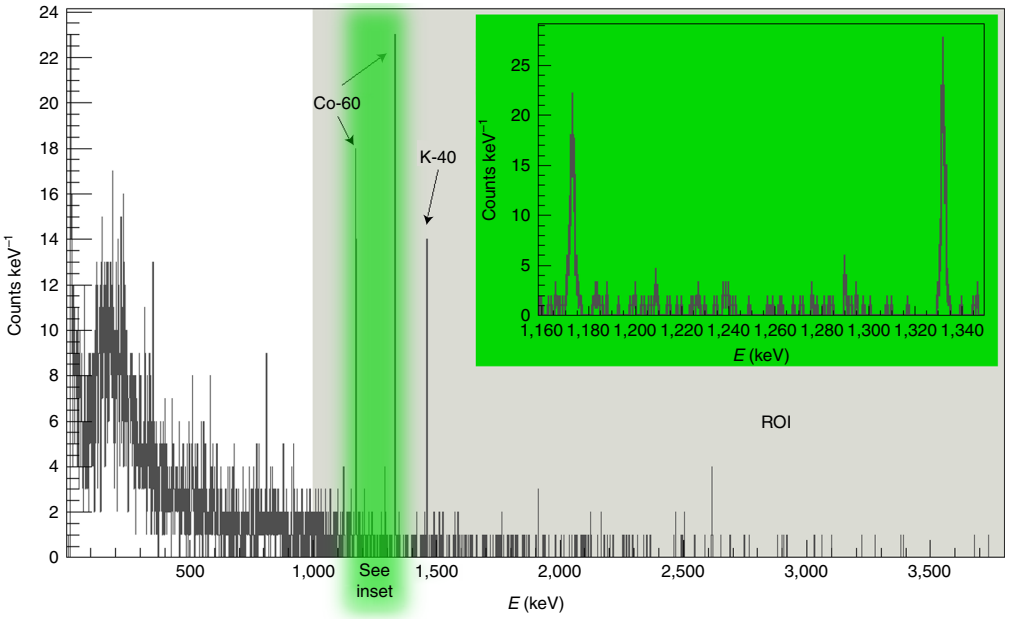

Fig. 3 | Measured radiation spectrum. The measured emission spectrum, corresponding to a data-taking period of about 62 days, is represented as a dark-grey histogram. The natural binning of 1 keV is used; the bin contents are shown without error bars, in order to appreciate the relative intensities of the residual radionuclide emission lines. The ^{60}Co and ^{40}K lines are also indicated. Inset: magnification of the region of the ^{60}Co lines (which is highlighted in the total plot by the shaded green area); here the error bars are shown and represent 1 s.d. The grey area shows the ROI, which is defined as $\Delta E = (1{,}000\text{–}3{,}800)$ keV.

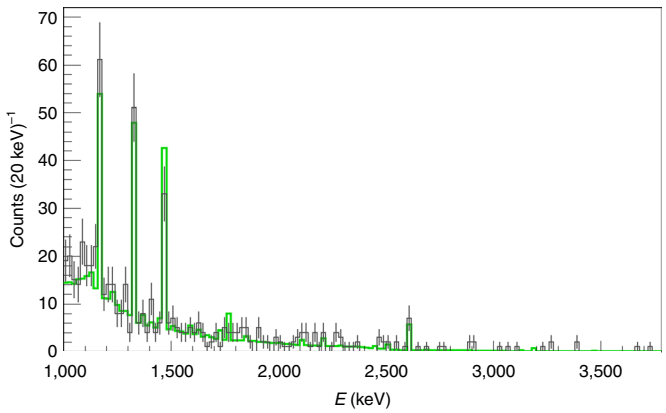

Fig. 4 | Comparison between the measured and the simulated background spectra. The measured emission spectrum is shown in the ROI as a dark-grey histogram, with error bars representing 1 s.d. The simulated background distribution is shown in green for comparison. The simulation is based on a Geant4 validated MC characterization of the whole detector. The MC has as input the measured activities of the residual radionuclides for each material present in the experimental set-up. The simulation accounts for the emission probabilities and the decay schemes, the photon propagation and interactions in the materials of the apparatus and the detection efficiencies (Methods).

It is important to stress that the energy range in which spontaneous photon emission is expected extends from the upper threshold of the detector sensitive region (3.8 MeV) to 100 MeV (according to the emission rate given in equation (4)). A fraction of these primary photons could be degraded in energy due to Compton scattering, thus producing additional events in the ROI. Such a process would result in a stronger lower bound on R_0. We made an estimate of the improvement (I) on the bound by considering the limiting case in which all the primary spontaneously emitted photons generated in the ith component of the set-up, in the energy range (3.8–100) MeV, are degraded, due to scattering, to the energy $E_i^{\max,\,\mathrm{eff}}$ within the ROI, corresponding to the maximal detection efficiency for the ith material. We obtain $I \sim 1.620$, which is not sizable (even under the exaggerated assumptions we considered); this is mainly due to the fact that spontaneous emission decreases with energy as $1/E$.

Our experiment sets a lower bound on R_0 of the order of 1 Å, which is about three orders of magnitude stronger than previous bounds in the literature[36,42]; see Fig. 5. If R_0 is the size of the nucleus's wave function as suggested by Penrose, we have to confront our result with known properties of nuclei in matter. In a crystal, $R_0 = \sqrt{\langle u^2 \rangle}$ where $\langle u^2 \rangle$ is the mean square displacement of a nucleus in the lattice, which can be computed by using the relation[43,44] $\langle u^2 \rangle = B/8\pi^2$, where $B = 0.20$ Å^2 is the Debye–Waller factor for the germanium crystal[45], cooled to liquid nitrogen temperature. One obtains $R_0 = 0.05 \times 10^{-10}$ m, which is more than an order of magnitude smaller than the lower limit set by our experiment. Therefore, we conclude that Penrose's proposal for a gravity-related collapse of the wave function, in the present formulation, is ruled out.

Of course, alternatives are always possible. Following Diósi, one option is to leave R_0 completely free; however, this comes at the price of having a parameter whose value is unjustified, apparently disconnected from the mass density of the system as well as from gravitational effects. Another option is to change the way the collapse is modelled (Poissonian decay), thereby adding extra terms and parameters to take into account a more complex dynamics, as done for other collapse models[46–48]. This kind of extension has not been envisaged in the literature so far. Our result indicates that the idea of gravity-related wave function collapse, which remains very appealing, will probably require a radically new approach.

Online content

Any methods, additional references, Nature Research reporting summaries, source data, extended data, supplementary information,

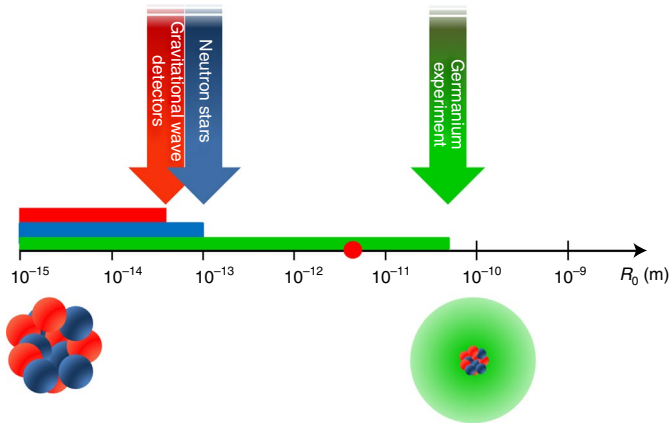

Fig. 5 | Lower bounds on the spatial cutoff R_0 of the DP model. According to Penrose, $R_0 = 0.05 \times 10^{-10}$ m for the germanium crystal used in the experiment (red circle on the horizontal scale). Our experiment sets a lower bound on R_0 at 0.54×10^{-10} m (green bar and arrow), which is one order of magnitude larger than predicted following Penrose's argument. Therefore, this parameter-free version of the DP model is excluded. The figure shows also previous lower bounds in the literature, similarly based on the monitoring of the Brownian-like diffusion predicted by the DP model. They refer to data analysis from gravitational wave detectors[36] ($R_0 \geq (40.1 \pm 0.5) \times 10^{-15}$ m, red bar and arrow) and neutron stars[42] ($R_0 \gtrsim 10^{-13}$ m, blue bar and arrow). The figure shows the range of hypothetical values of R_0, from the size of a nucleus (red-blue cluster) to beyond that of an atom (green halo surrounding the red-blue nucleus).

acknowledgements, peer review information; details of author contributions and competing interests; and statements of data and code availability are available at https://doi.org/10.1038/s41567-020-1008-4.

Received: 25 November 2019; Accepted: 17 July 2020;
Published online: 07 September 2020

References

1. Schrödinger, E. Die gegenwärtige Situation in der Quantenmechanik. *Naturwissenschaften* **23**, 823–828 (1935).
2. Leggett, A. J. Macroscopic quantum systems and the quantum theory of measurement. *Prog. Theor. Phys. Suppl.* **69**, 80–100 (1980).
3. Weinberg, S. Precision tests of quantum mechanics. *Phys. Rev. Lett.* **62**, 485–488 (1989).
4. Bell, J. S. *Speakable and Unspeakable in Quantum Mechanics: Collected Papers on Quantum Philosophy* (Cambridge Univ. Press, 2004).
5. Ghirardi, G. C., Rimini, A. & Weber, T. Unified dynamics for microscopic and macroscopic systems. *Phys. Rev. D* **34**, 470–491 (1986).
6. Adler, S. L. *Quantum Theory as an Emergent Phenomenon: the Statistical Mechanics of Matrix Models as the Precursor of Quantum Field Theory* (Cambridge Univ. Press, 2004).
7. Weinberg, S. Collapse of the state vector. *Phys. Rev. A* **85**, 062116 (2012).
8. Ghirardi, G. C., Pearle, P. & Rimini, A. Markov processes in Hilbert space and continuous spontaneous localization of systems of identical particles. *Phys. Rev. A* **42**, 78–89 (1990).
9. Bassi, A. & Ghirardi, G. Dynamical reduction models. *Phys. Rep.* **379**, 257–426 (2003).
10. Bassi, A., Lochan, K., Satin, S., Singh, T. P. & Ulbricht, H. Models of wave-function collapse, underlying theories, and experimental tests. *Rev. Mod. Phys.* **85**, 471–527 (2013).
11. Arndt, M. & Hornberger, K. Testing the limits of quantum mechanical superpositions. *Nat. Phys.* **10**, 271–277 (2014).
12. Feynman, R. *Feynman Lectures on Gravitation* (CRC Press, 2018).
13. Penrose, R. & Mermin, N. D. *The Emperor's New Mind: Concerning Computers, Minds, and the Laws of Physics* (Oxford Univ. Press, 1990).
14. Penrose, R. On gravity's role in quantum state reduction. *Gen. Relativ. Gravit.* **28**, 581–600 (1996).
15. Penrose, R. On the gravitization of quantum mechanics 1: Quantum state reduction. *Found. Phys.* **44**, 557–575 (2014).
16. Howl, R., Penrose, R. & Fuentes, I. Exploring the unification of quantum theory and general relativity with a Bose–Einstein condensate. *New J. Phys.* **21**, 043047 (2019).
17. Diósi, L. A universal master equation for the gravitational violation of quantum mechanics. *Phys. Lett. A* **120**, 377–381 (1987).
18. Diósi, L. Models for universal reduction of macroscopic quantum fluctuations. *Phys. Rev. A* **40**, 1165–1174 (1989).
19. Ghirardi, G., Grassi, R. & Rimini, A. Continuous-spontaneous-reduction model involving gravity. *Phys. Rev. A* **42**, 1057–1064 (1990).
20. Diósi, L. Gravity-related wave function collapse: mass density resolution. *J. Phys. Conf. Ser.* **442**, 012001 (2013).
21. Diósi, L. Gravitation and quantum-mechanical localization of macro-objects. *Phys. Lett. A* **105**, 199–202 (1984).
22. Bahrami, M., Großardt, A., Donadi, S. & Bassi, A. The Schrödinger–Newton equation and its foundations. *New J. Phys.* **16**, 115007 (2014).
23. Salart, D., Baas, A., van Houwelingen, J. A., Gisin, N. & Zbinden, H. Spacelike separation in a Bell test assuming gravitationally induced collapses. *Phys. Rev. Lett.* **100**, 220404 (2008).
24. Marshall, W., Simon, C., Penrose, R. & Bouwmeester, D. Towards quantum superpositions of a mirror. *Phys. Rev. Lett.* **91**, 130401 (2003).
25. Kovachy, T. et al. Quantum superposition at the half-metre scale. *Nature* **528**, 530–533 (2015).
26. Fein, Y. Y. et al. Quantum superposition of molecules beyond 25 kDa. *Nat. Phys.* **15**, 1242–1245 (2019).
27. Lee, K. C. et al. Entangling macroscopic diamonds at room temperature. *Science* **334**, 1253–1256 (2011).
28. Chan, J. et al. Laser cooling of a nanomechanical oscillator into its quantum ground state. *Nature* **478**, 89–92 (2011).
29. Teufel, J. et al. Sideband cooling of micromechanical motion to the quantum ground state. *Nature* **475**, 359–363 (2011).
30. Wollman, E. E. et al. Quantum squeezing of motion in a mechanical resonator. *Science* **349**, 952–955 (2015).
31. Jain, V. et al. Direct measurement of photon recoil from a levitated nanoparticle. *Phys. Rev. Lett.* **116**, 243601 (2016).
32. Hong, S. et al. Hanbury Brown and Twiss interferometry of single phonons from an optomechanical resonator. *Science* **358**, 203–206 (2017).
33. Vovrosh, J. et al. Parametric feedback cooling of levitated optomechanics in a parabolic mirror trap. *J. Opt. Soc. Am. B* **34**, 1421–1428 (2017).
34. Riedinger, R. et al. Remote quantum entanglement between two micromechanical oscillators. *Nature* **556**, 473–477 (2018).
35. Bahrami, M., Smirne, A. & Bassi, A. Role of gravity in the collapse of a wave function: a probe into the Diósi–Penrose model. *Phys. Rev. A* **90**, 062105 (2014).
36. Helou, B., Slagmolen, B., McClelland, D. E. & Chen, Y. LISA Pathfinder appreciably constrains collapse models. *Phys. Rev. D* **95**, 084054 (2017).
37. Diósi, L. & Lukács, B. Calculation of X-ray signals from Károlyházy hazy space-time. *Phys. Lett. A* **181**, 366–368 (1993).
38. Neder, H., Heusser, G. & Laubenstein, M. Low level γ-ray germanium-spectrometer to measure very low primordial radionuclide concentrations. *Appl. Radiat. Isot.* **53**, 191–195 (2000).
39. Heusser, G., Laubenstein, M. & Neder, H. Low-level germanium gamma-ray spectrometry at the μBq/kg level and future developments towards higher sensitivity. *Radioact. Environ.* **8**, 495–510 (2006).
40. Fu, Q. Spontaneous radiation of free electrons in a nonrelativistic collapse model. *Phys. Rev. A* **56**, 1806–1811 (1997).
41. Piscicchia, K. et al. CSL collapse model mapped with the spontaneous radiation. *Entropy* **19**, 319 (2017).
42. Tilloy, A. & Stace, T. M. Neutron star heating constraints on wave-function collapse models. *Phys. Rev. Lett.* **123**, 080402 (2019).
43. Debye, P. Interferenz von Röntgenstrahlen und Wärmebewegung. *Ann. Phys.* **348**, 49–92 (1913).
44. Waller, I. Zur Frage der Einwirkung der Wärmebewegung auf die Interferenz von Röntgenstrahlen. *Z. Phys.* **17**, 398–408 (1923).
45. Gao, H. & Peng, L.-M. Parameterization of the temperature dependence of the Debye–Waller factors. *Acta Crystallogr. A* **55**, 926–932 (1999).
46. Adler, S. L. & Bassi, A. Collapse models with non-white noises. *J. Phys. A* **40**, 15083 (2007).
47. Adler, S. L. & Bassi, A. Collapse models with non-white noises: II. Particle-density coupled noises. *J. Phys. A* **41**, 395308 (2008).
48. Gasbarri, G., Toroš, M., Donadi, S. & Bassi, A. Gravity induced wave function collapse. *Phys. Rev. D* **96**, 104013 (2017).

Methods

Calculation of the radiation emission rate. We summarize the main steps for deriving equation (4) for the emission rate of the main text. The starting point is the quantum mechanical formula for the radiation emission rate

$$\frac{\mathrm{d}}{\mathrm{d}\omega_k}\Gamma_t = \frac{k^2}{c}\sum_\nu \int \mathrm{d}\Omega_k \frac{\mathrm{d}}{\mathrm{d}t}\langle a^\dagger_{\mathbf{k}\nu} a_{\mathbf{k}\nu}\rangle_t \tag{7}$$

where $\langle a^\dagger_{\mathbf{k}\nu} a_{\mathbf{k}\nu}\rangle_t$ gives the average number of photons emitted at time t with wave vector $\mathbf{k}$ and polarization ν. The time derivative accounts for the fact that we are computing a rate; the integration over the solid angle Ω_k, and polarizations of the photons for the fact that we are interested in the total number of photons emitted in a given energy range, independently from these degrees of freedom; and the factor $\frac{k^2}{c}$ for the density of wave vectors with modulus k.

The expectation value $\langle a^\dagger_{\mathbf{k}\nu} a_{\mathbf{k}\nu}\rangle_t$ is computed starting from the master equation (3) of the main text, which it is convenient to rewrite in the following form[35]:

$$\begin{aligned}\tfrac{\mathrm{d}\rho(t)}{\mathrm{d}t} &= -\tfrac{i}{\hbar}[H,\rho(t)] + \int \mathrm{d}\mathbf{Q}\sum_{n,n'}\tilde{\Gamma}_{n,n'}(\mathbf{Q}) \\ &\left(\mathrm{e}^{\frac{i}{\hbar}\mathbf{Q}\cdot\mathbf{x}_n}\rho(t)\,\mathrm{e}^{-\frac{i}{\hbar}\mathbf{Q}\cdot\mathbf{x}_{n'}} - \tfrac{1}{2}\left\{\mathrm{e}^{-\frac{i}{\hbar}\mathbf{Q}\cdot\mathbf{x}_{n'}}\,\mathrm{e}^{\frac{i}{\hbar}\mathbf{Q}\cdot\mathbf{x}_n},\rho(t)\right\}\right)\end{aligned} \tag{8}$$

where $\mathbf{Q}$ is an integration variable with the dimension of momentum, $\mathbf{x}_n$ is the position operator of the n-th particle, and

$$\tilde{\Gamma}_{n,n'}(\mathbf{Q}) = \frac{4G}{\pi\hbar^2}\frac{\tilde{\mu}_n(\mathbf{Q})\tilde{\mu}^*_{n'}(\mathbf{Q})}{Q^2} \tag{9}$$

with

$$\tilde{\mu}(\mathbf{Q}) = \frac{1}{2\pi\hbar^3}\int \mathrm{d}\mathbf{y}\,\mu(\mathbf{y})\,\mathrm{e}^{-\frac{i}{\hbar}\mathbf{Q}\cdot\mathbf{y}} \tag{10}$$

the Fourier transform of the mass density $\mu(\mathbf{y})$.

We move to the Heisenberg picture, introducing the adjoint master equation of equation (8), which for a generic operator O takes the form[49]

$$\begin{aligned}\tfrac{\mathrm{d}}{\mathrm{d}t}O(t) &= \tfrac{i}{\hbar}[H,O(t)] + \int \mathrm{d}\mathbf{Q}\sum_{k,k'}\tilde{\Gamma}_{k,k'}(\mathbf{Q}) \\ &\left(\mathrm{e}^{-\frac{i}{\hbar}\mathbf{Q}\cdot\mathbf{x}_{k'}}O(t)\,\mathrm{e}^{\frac{i}{\hbar}\mathbf{Q}\cdot\mathbf{x}_k} - \tfrac{1}{2}\left\{O(t),\mathrm{e}^{-\frac{i}{\hbar}\mathbf{Q}\cdot\mathbf{x}_{k'}}\,\mathrm{e}^{\frac{i}{\hbar}\mathbf{Q}\cdot\mathbf{x}_k}\right\}\right)\end{aligned} \tag{11}$$

H is the sum of three contributions:

$$H = H_\mathrm{S} + H_\mathrm{R} + H_\mathrm{INT} \tag{12}$$

The first term is

$$H_\mathrm{S} = \sum_j\left(\frac{\mathbf{p}_j^2}{2m_j} + V(\mathbf{x}_j) + \sum_{i<j}U(\mathbf{x}_j-\mathbf{x}_i)\right) \tag{13}$$

where the sums run over all particles of the system; V is an external potential and U the potential among the particles of the system. We focus on the emission from a crystal; therefore, the sum will run over all the electrons and the nuclei of the system (given the energy range of the emitted photons we consider, we do not need to resolve the internal structure of the nuclei by considering their protons). The free electromagnetic Hamiltonian is

$$H_\mathrm{R} = \sum_\nu\int \mathrm{d}\mathbf{k}\,\hbar\omega_k\left(\frac{1}{2} + a^\dagger_{\mathbf{k},\nu}a_{\mathbf{k},\nu}\right) \tag{14}$$

where $\omega_k = kc$ and $a_{\mathbf{k},\nu}$, $a^\dagger_{\mathbf{k},\nu}$ are, respectively, the annihilation and creation operators of a photon with wave vector $\mathbf{k}$ and polarization ν. The last term describes the usual interaction between the electromagnetic field and the particles (at the non-relativistic level):

$$H_\mathrm{INT} = \sum_j\left(-\frac{e_j}{m_j}\right)\mathbf{A}(\mathbf{x}_j)\cdot\mathbf{p}_j + \sum_j\frac{e_j^2}{2m_j}\mathbf{A}^2(\mathbf{x}_j) \tag{15}$$

where e_j and m_j are the charge and the mass of the jth particle of the system and $\mathbf{A}(\mathbf{x})$ is the vector potential, which can be expanded in plane waves as

$$\mathbf{A}(\mathbf{x}) = \int \mathrm{d}\mathbf{k}\sum_\nu\alpha_k\left[\boldsymbol{\varepsilon}_{\mathbf{k},\nu}\,a_{\mathbf{k},\nu}\,\mathrm{e}^{i\mathbf{k}\cdot\mathbf{x}} + \boldsymbol{\varepsilon}_{\mathbf{k},\nu}\,a^\dagger_{\mathbf{k},\nu}\,\mathrm{e}^{-i\mathbf{k}\cdot\mathbf{x}}\right] \tag{16}$$

with $\alpha_k = [\hbar/2\varepsilon_0\omega_k(2\pi)^3]^{1/2}$, $\boldsymbol{\varepsilon}_{\mathbf{k},\nu}\cdot\mathbf{k} = 0$ and $\boldsymbol{\varepsilon}_{\mathbf{k},\nu}$ the (real) polarization vectors. Note that in equation (15) the term proportional to $\mathbf{p}_j\cdot\mathbf{A}(\mathbf{x}_j)$ is missing because we are working in the Coulomb gauge where $\nabla\cdot\mathbf{A} = 0$, implying $\boldsymbol{\varepsilon}_{\mathbf{k},\nu}\cdot\mathbf{k} = 0$; therefore, this term contributes in the same way as the term $\mathbf{A}(\mathbf{x}_j)\cdot\mathbf{p}_j$ and the two can be added.

Starting from equation (11), $\langle a^\dagger_{\mathbf{k}\nu}a_{\mathbf{k}\nu}\rangle_t$ is computed and then inserted in equation (7) to find the rate. The calculation is long but conceptually simple: the integral form of equation (11) is expanded perturbatively up to the second order (the first-order terms give no contribution), similarly to what is usually done when the evolution operator is expanded using the Dyson series. Then one has to compute the nine terms resulting from this expansion. The calculation is fully reported in Supplementary Information; here we give the physical picture underlying the calculations, which proved to be successful when applied to other models of spontaneous wave function collapse[40,50–53].

We can understand the mechanism of radiation emission in terms of a semiclassical picture. Each time there is a collapse, particles are 'kicked', corresponding to an acceleration with associated radiation emission. The radiation emitted from different particles may add coherently or incoherently, and to understand under which conditions these occur it is instructive to study the radiation emission from two charged particles in the context of classical electrodynamics.

Suppose the two particles are accelerated by the same external force. At a point x very far away from the charges, the values of the emitted radiation crucially depends both on the distance L between the particles and the wavelength λ of the emitted radiation. If the charges have opposite signs, when $L \ll \lambda$, given $x \gg L,\lambda$, the electric fields $E_1(x)$ generated by the positive charge and $E_2(x)$ generated by the negative charge will be the same, just with opposite sign, due to the opposite value of the charges. Then in this case $E_\mathrm{tot}(x) = E_1(x) + E_2(x) \simeq 0$, and because the emitted radiation is proportional to $|E_\mathrm{tot}(x)|^2$ there is almost a full cancellation of the radiation field. In contrast, if both charges have the same sign, $E_\mathrm{tot}(x) = E_1(x) + E_2(x) \simeq 2E_1(x)$, hence the emitted radiation becomes four times larger than that emitted by a single charge. In more informal terms, we can say that for $L \ll \lambda$ a detector at x sees the charges as if they are sitting at the same point. This leads to a coherent emission, which suppresses the radiation emitted when the particles have opposite charges and maximizes it when they have the same charge.

On the other hand, let us now consider the case $L \gg \lambda$. Still assuming $x \gg L,\lambda$, the two electric fields $E_1(x)$ and $E_2(x)$ have in general different intensities. In fact, if we label by x_1 (x_2) the distance between the point x and the point where the first (second) particle is located, we have $|x_1 - x_2| \sim L$. Then the electric fields oscillate many times in the distance $|x_1 - x_2|$. Therefore, even if at a given point x they perfectly cancel, at a nearby point $x + \mathrm{d}x$ they add constructively. As for the intensity, one has $I(x) \propto |E_\mathrm{tot}(x)|^2 = |E_1(x)|^2 + |E_2(x)|^2 + E_1^*(x)E_2(x) + E_1(x)E_2^*(x)$, and when we integrate over a spherical surface of radius $|x|$, to find the total emission rate, the last two terms average to zero due to the fast oscillating behaviour, and we obtain that the two particles emit independently.

Going back to the calculation in the main text, since the distance between electrons and nuclei is of the order of 1 Å, while the wavelength of the photons we are considering in the experiment is much smaller ($3.3\times10^{-3} < \lambda < 1.2\times10^{-2}$ Å), we are precisely in the second situation described above, so electrons and nuclei emit independently. In contrast, protons in the same nucleus are much closer than the smallest wavelength of the photons we are considering, which explains why they emit coherently. As a result, the emission rate from the crystal is given by equation (4) of the main text, where the emission from the electrons is neglected and the incoherent emission from all atoms in the crystal is considered.

As a final note, in the DP model there is another reason for the incoherent radiation by electrons and nuclei, as long as $R_0 \ll L$ (which holds in our case). The gravitational fluctuations, underlying the decoherence term of equation (3), which accelerate the charges, become uncorrelated beyond the range R_0: the electrons and the nuclei are accelerated by uncorrelated kicks, resulting in an induced incoherent emission.

Statistical analysis. Each component of the experimental apparatus was characterized by means of MC simulations[54] based on the Geant4 software library (verified by participating in international proficiency tests organized by the IAEA). The simulations were used to determine (1) the expected background due to residual radionuclides in the materials of the set-up and (2) the expected spontaneous radiation emission contribution to the measured spectrum. More detail follows.

1. The MC simulation of the background is based on the measured activities of the residual radionuclides, in all the components of the set-up. The simulation accounts for the emission probabilities and the decay schemes, the photon propagation and interactions in the materials of the apparatus, and the detection efficiencies. The obtained spectrum is compared with the measured distribution in Fig. 4.
2. The efficiency, as a function of the energy, for the detection of spontaneously emitted photons was obtained by generating 10^8 photons, for each component of the set-up, in steps of 200 keV (that is 15 points in the ROI $\Delta E = E_1 - E_2 = (1{,}000–3{,}800)$ keV). The $\epsilon_i(E)$ were then estimated from polynomial fits of the corresponding distributions. Given the rate in equation (4) one expects to measure a number of events

$$\int_{\Delta E}\left.\frac{\mathrm{d}\Gamma_t}{\mathrm{d}E}\right|_i T\epsilon_i(E)\,\mathrm{d}E \tag{17}$$

due to the spontaneous emission by protons belonging to the ith material during T. Summing over all the materials, the total signal contribution (see equation (5)) is obtained: $z_\mathrm{s}(R_0) = a/R_0^3$.

The stochastic variable, representing the total number of photon counts measured in the range ΔE, follows a Poisson distribution:

$$p(z_c|\Lambda_c) = \frac{\Lambda_c^{z_c}\, e^{-\Lambda_c}}{z_c!} \tag{18}$$

with Λ_c the corresponding expected value. Two sources contribute to the measured spectrum: a background (b) originated by all known emission processes, together with a potential signal (s) due to spontaneously emitted photons induced by the collapse process. The total number of counts, respectively z_b and z_s, that would be measured in the period T were estimated according to steps (1) and (2). The corresponding independent stochastic variables can be also associated with Poisson distributions, whose expected values (Λ_b and Λ_s) are then related by

$$\Lambda_c(R_0) = \Lambda_b + \Lambda_s(R_0) = z_b + z_s(R_0) + 2 \tag{19}$$

where the dependence on R_0 is explicitly shown.

The pdf of $\Lambda_c(R_0)$ can then be obtained from equation (18) by applying the Bayes theorem:

$$\tilde{p}(\Lambda_c(R_0)|p(z_c|\Lambda_c(R_0))) = \frac{p(z_c|\Lambda_c(R_0)) \cdot \tilde{p}_0(\Lambda_c(R_0))}{\int_D p(z_c|\Lambda_c(R_0)) \cdot \tilde{p}_0(\Lambda_c(R_0))\, d[\Lambda_c(R_0)]} \tag{20}$$

with D the domain of Λ_c and $\tilde{p}_0$ the prior distribution. R_0 is constrained by the requirement $R_0 > R_0^{min} = 10^{-14}$ m, which implies an upper bound on Λ_c (see equation (19)). We then used a Heaviside function for the prior

$$\tilde{p}_0(\Lambda_c(R_0)) = \theta(\Lambda_c^{max} - \Lambda_c(R_0)) \tag{21}$$

with $\Lambda_c^{max} = \Lambda_c(R_0^{min})$. From equation (20) the pdf of $\Lambda_c(R_0)$ is

$$\tilde{p}(\Lambda_c(R_0)) = \frac{\Lambda_c^{z_c}\, e^{-\Lambda_c}\, \theta(\Lambda_c^{max} - \Lambda_c)}{\int_0^{\Lambda_c^{max}} \Lambda_c^{z_c}\, e^{-\Lambda_c}\, d\Lambda_c} \tag{22}$$

In order to obtain the bound given in equation (6) we then have to solve the following integral equation for the cumulative pdf:

$$\tilde{P}(\bar{\Lambda}_c) = \frac{\gamma(z_c + 1, \bar{\Lambda}_c)}{\gamma(z_c + 1, \Lambda_c^{max})} = 0.95 \tag{23}$$

which yields $\Lambda_c < \bar{\Lambda}_c = 617$. As a consequence

$$\Lambda_c(R_0) = \Lambda_s(R_0) + \Lambda_b < 617 \Rightarrow \frac{a}{R_0^3} + \Lambda_b + 1 < 617 \Rightarrow R_0 > \left(\frac{a}{616 - \Lambda_b}\right)^{1/3} \tag{24}$$

The analysis was performed in the energy range E_1–E_2 in which all the hypotheses of the model, for the spontaneous emission of protons, are fulfilled. However, the energy range in which spontaneous photon emission is expected, according to equation (4), extends up to 100 MeV. A fraction of spontaneously emitted photons with energy $E \in E_2$–$E_3 = (3.8$–$100)$ MeV could be degraded in energy due to Compton scattering, thus contributing to $\Lambda_s(R_0)$; for this reason we estimated the corresponding I to the bound in equation (6). Any improvement in the description of the expected background (or signal) contribution would lead to a larger value of Λ_b (or a), and from equation (24) one can infer that this would translate into a stronger bound on R_0.

Regarding Λ_b, since the MC simulation is based on the measured activities, we do not expect a contribution to photon emission, at energies higher than 3.8 MeV, originating from radionuclide decays.

The total number of spontaneously emitted photons that are generated in the materials of the detector in the energy range E_2–E_3 is given by

$$\sum_i \int_{E_2}^{E_3} \left|\frac{d\Gamma_t}{dE}\right|_i T\, dE = \sum_i \int_{E_2}^{E_3} N_i^2 N_{ai} \beta T \frac{1}{R_0^3 E}\, dE = \frac{b}{R_0^3} > 0 \tag{25}$$

where N_i and N_{ai} are, respectively, the number of protons contained in each atom and the number of atoms of the ith material, while the constant β is defined as

$$\beta = \frac{2}{3}\frac{Ge^2}{\pi^{3/2}\varepsilon_0 c^3} \tag{26}$$

Let us denote by f the fraction of these photons which, due to Compton scattering, produce events in the ROI and are detected. The total signal contribution then turns out to be

$$z_s(R_0) = \frac{a}{R_0^3} + \frac{fb}{R_0^3} > \frac{a}{R_0^3} \tag{27}$$

Since $a + fb > a$, the contribution of the spontaneous emission in the range E_2–E_3 improves the bound on R_0 by a factor $[(a + fb)/a]^{1/3}$.

We extracted the maximal I under the extreme—nonetheless most conservative—assumption that all the primary spontaneously emitted photons generated in the ith material, in the energy range E_2–E_3, are degraded, due to scattering, to the energy $E_i^{max,\,eff} \in E_1$–E_2, which corresponds to the maximal efficiency for the corresponding material (see Supplementary Fig. 1). The total signal contribution then amounts to

$$\begin{aligned} z_s(R_0) = {} & \sum_i \int_{E_1}^{E_2} \left|\frac{d\Gamma_t}{dE}\right|_i T \epsilon_i(E)\, dE + \sum_i \epsilon_i^{max} \int_{E_2}^{E_3} \left|\frac{d\Gamma_t}{dE}\right|_i T\, dE \\ = {} & ((1.756 + 5.712) \times 10^{-29}) \frac{m^3}{R_0^3} = \frac{a + fb}{R_0^3} \end{aligned} \tag{28}$$

which corresponds to $I \sim 1.620$. The improvement is not sizable, as stated in the main text, even under the exaggerated assumptions we considered.

Data availability

Source data are provided with this paper. All other data that support the plots within this paper and other findings of this study are available from the corresponding author upon reasonable request.

Code availability

The MC simulation is based on Geant4 code, which is freely accessible at http://geant4.web.cern.ch/support/download. Experimental details used within the simulation code as part of this study are protected by a non-disclosure agreement with the manufacturing company, but the results of the simulation are available for this paper.

References

49. Breuer, H. P. & Petruccione, F. *The Theory of Open Quantum Systems* (Oxford Univ. Press, 2002).
50. Adler, S. L. & Ramazanoglu, F. M. Photon-emission rate from atomic systems in the CSL model. *J. Phys. A* **40**, 13395 (2007).
51. Adler, S. L., Bassi, A. & Donadi, S. On spontaneous photon emission in collapse models. *J. Phys. A* **46**, 245304 (2013).
52. Bassi, A. & Donadi, S. Spontaneous photon emission from a non-relativistic free charged particle in collapse models: a case study. *Phys. Lett. A* **378**, 761–765 (2014).
53. Donadi, S., Deckert, D.-A. & Bassi, A. On the spontaneous emission of electromagnetic radiation in the CSL model. *Ann. Phys.* **340**, 70–86 (2014).
54. Boswell, M. et al. Mage—a Geant4-based Monte Carlo application framework for low-background germanium experiments. *IEEE Trans. Nucl. Sci.* **58**, 1212–1220 (2011).

Acknowledgements

We thank S. L. Adler, M. Arndt and H. Ulbricht for useful discussions and comments, and C. Capoccia, M. Carlesso and R. Del Grande for their help in preparing the figures. S.D. acknowledges support from The Foundation BLANCEFLOR Boncompagni Ludovisi, née Bildt, INFN and the Fetzer Franklin Fund. K.P. and C.C. acknowledge the support of the Centro Fermi—Museo Storico della Fisica e Centro Studi e Ricerche 'Enrico Fermi' (Open Problems in Quantum Mechanics project), the John Templeton Foundation (ID 58158) and FQXi. L.D. acknowledges the support of the National Research Development and Innovation Office of Hungary, grant nos. 2017-1.2.1-NKP-2017-00001 and K12435, and support by an FQXi minigrant. A.B. acknowledges support from the H2020 FET TEQ (grant no. 766900), the University of Trieste and INFN. All authors acknowledge support from the COST Action QTSpace (grant no. CA15220).

Author contributions

S.D. and A.B. conceived and designed the theoretical aspects of the research; M.L., K.P. and C.C. designed the experimental part of the research; S.D. performed the theoretical calculations, with the assistance of A.B. and L.D.; M.L., K.P. and C.C. performed the experimental measurements; K.P. performed the data analysis, with the assistance of C.C., M.L. and L.D.; S.D., K.P. and A.B. prepared the manuscript and Supplementary Information in coordination with all authors.

Competing interests

The authors declare no competing interests.

Additional information

Supplementary information is available for this paper at https://doi.org/10.1038/s41567-020-1008-4.

Correspondence and requests for materials should be addressed to S.D., K.P. or A.B.

Reprints and permissions information is available at www.nature.com/reprints.